Multilevel Spherical Photonic Crystals with Controllable Structures and

Structure-Enhanced Functionalities

Juan Wang[a,b], Hai Le-The[b,c], Lingling Shui*[,a,d], Johan G. Bomer[b], Mingliang Jin[a,d], Guofu Zhou[a,d], Paul Mulvaney[d,e], Pepijn W. H. Pinkse[f], Albert van den Berg[b], Loes I. Segerink[b], and Jan C. T. Eijkel[b]

[a]National Centre for International Research on Green Optoelectronics, South China Academy of Advanced Optoelectronics & School of Information Optoelectronic Science and Engineering, South China Normal University, 510006 Guangzhou, China.

[b]BIOS Lab-on-a-Chip Group, MESA+ Institute for Nanotechnology, Technical Medical Centre & Max Planck Centre for Complex Fluid Dynamics, University of Twente, 7500 AE Enschede, the Netherlands.

[c]Physics of Fluids Group, MESA+ Institute for Nanotechnology & Max Planck Center for Complex Fluid Dynamics, University of Twente, 7500 AE Enschede, the Netherlands.

[d]International Academy of Optoelectronics at Zhaoqing, South China Normal University, 510631 Guangzhou, China.

[e]ARC Centre of Excellence in Exciton Science, School of Chemistry, University of Melbourne, 3010, Parkville, VIC., Australia.

[f]Complex Photonic Systems Group, MESA+ Institute for Nanotechnology, University of Twente, 7500 AE Enschede, the Netherlands.

shuill@m.scnu.edu.cn

ABSTRACT

This is the author manuscript accepted for publication and has undergone full peer review but has not been through the copyediting, typesetting, pagination and proofreading process, which may lead to differences between this version and the Version of Record. Please cite this article as doi: 10.1002/adom.201902164.

Spherical photonic crystals (SPCs) with tailorable multi-scale structure, versatile surface morphology, and controllable optical properties of both photonic stop band (PSB) and surface plasmon resonance (SPR), have been fabricated using a robust and facile method. The fabricated SPCs consist of well-spaced gold nanocrystals (AuNCs) (3^{rd}-tier) anchored on silica nanopatterns (2^{nd}-tier) confined in microspherical templates (1^{st}-tier). Droplet microfluidics is used to produce microdroplets containing silica nanoparticles (SiO_2NPs) which assemble to form two-tier SPCs. Subsequently, three-tier SPCs are obtained by thermal dewetting and evaporation of metal films deposited on the two-tier SPCs, with the 3^{rd}-tier morphology being controlled by the deposited film morphology and programmed thermal annealing. Optical PSB and SPR properties of the prepared SPCs can be on-demand tailored by the 2^{nd} and -3^{rd}-tier morphology and their corresponding constituent materials. We find that the scattering from AuNC arrays on the SPCs can be amplified by tailoring the PSB properties. The hierarchical SPCs manufactured by this method takes advantages of low-cost, high controllability and further processability. We have demonstrated the manufacturing of flexible films encapsulated well-assembled SPCs as anticounterfeiting stamps, which are easy to be identified using the mobile phone with a flash.

Keywords: spherical photonic crystal (SPC), droplet microfluidics, dewetting, periodic lattice, photonic stop band (PSB), surface plasmon resonance (SPR)

1. Introduction

Hierarchical structures with different length scales and/or multilevel patterns created by microscale patterning can improve the mechanical properties of materials including strength, stability, and flexibility, while nanoscale structuring can lead to augmented functionalities in optics (*e.g.* reflection, antireflection, diffraction, and scattering),[1–3] physics (*e.g.*

superwetting and directional adhesion),[4–7] and even biology (*e.g.* tissue scaffolds).[8–11] Therefore application of these structures can be found in photonics,[12] electronics,[13] biology,[14] and catalysis.[15]

In particular, photonic crystals (PCs) possess periodic arrangements (on the order of the wavelength of light) of materials with different dielectric constants, being able to prevent light from propagating in certain directions at certain frequencies.[16,17] As a result, they can create a photonic stop band (PSB),[18] showing diverse structural colors. They have been used for manipulation, confinement, and control of light in three dimensions of space,[19] being useful in bio-inspired coloring,[20] photocatalysis,[21] chemical and biological sensors,[22,23] and reflective displays.[24] Slow light propagation is another specific property of these PCs.[25] Light can propagate with extremely reduced group velocities in the vicinity of the PSB,[25] thereby enhancing non-linear optical interactions,[25] sensor efficiencies,[22] and photochemical activity of the materials.[26]

Generally, PCs in two- or three-dimensional periodicity have been fabricated via a top-down approach[27,28] (*e.g.* soft lithography) or a bottom-up approach[19],[29] (*e.g.* colloid assembly). However, two-dimensional PC structures have angle dependent PSB limitations when compared to the spherical photonic crystals (SPCs) with high symmetric structure in three-dimension (3D). SPCs consist of periodically arranged nanostructures confined in microspheres with 3D symmetric property, and possess the advantage of a wide viewing angle which broadens their application area, for example, in optical materials/devices.[23,30] In the past decade, droplet microfluidics has been developed to a powerful tool for fabricating 3D SPCs[31,32] with high uniformity and controllable structures by combining top-down droplet generation with bottom-up self-assembly of colloids. The produced uniform microdroplets will act as curved templates that offer precise control over the layers of the

assembled building blocks and thereby the resulting PSB properties,[33] in contrast to the two-dimensional colloid assembly at the interface.[34]

Noble metal nanoparticles[35,36] have also been used as building blocks for SPCs construction due to their exceptional optical properties and applications in various fields, such as metamaterials, nanophotonics, and biotechnology.[37,38] Surface plasmon resonance (SPR) from noble metal nanoparticles originates from collective oscillation of conduction electrons when excited by electromagnetic radiation.[39] As a result, these noble metal nanoparticles can resonantly absorb and scatter light, showing vivid colors under dark field microscope.[40] The resulting colors depend on the shape and size of the nanoparticles and are influenced by the dielectric constant of the local surrounding medium as described by Mie scattering.[40] Noble metal nanoparticles have been applied in surface-enhanced Raman spectroscopy (amplified localized electromagnetic field),[41–43] biochemical sensors (high sensitivity to a change of the dielectric constant of the local environment),[44] and catalysis (free mobility of surface electrons).[45–47]

Although two-tier structures, for instance, core-satellite structures, consisting of organic (polystyrene particles) and inorganic particles (such as metal nanoparticles, silica nanoparticles (SiO_2NPs)) have been reported using either chemical methods[48,49] or physical methods,[50] a few works have reported on three-tier structures with high periodic arrangements consisting of both a 3D PC structure and a 2D metal array. Chu *et al.*[51] reported the fabrication of free-standing chiral plasmonic films, consisting of well-assembled rod-like cellulose nanocrystals with randomly infiltrated Au nanocrystals (AuNCs), which exhibited coupling of the PSB and SPR modes. Zhang *et al.*[52] reported a plasmonic material coupling a TiO_2-based PC substrate to AuNCs using anodization and a photocatalytic reduction method. However, in these cases the distribution of AuNCs on the PC structure was random, and the number density of AuNCs did not have a high reproducibility, especially

when a chemical method was followed. Thus, controllable patterning of plasmonic materials on PC structures with high uniformity and reproducibility is highly desired, allowing to achieve designed hierarchical periodical structures with amplified functionalities. The two-dimensional plasmonic arrays anchored on the top of PC structures also differs from the metal film coated two-tier PC microspheres, which showed obvious localized surface plasmon resonance (LSPR) resulted from the metal-covered sub-20 nm nanogaps.[31] In addition, patterning of plasmonic materials on PC structures takes advantages of further processability, such as functionalization and transfer the obtained structures from a hard substrate to a soft substrate to broaden their applications.

Therefore, in this work, we report a robust and facile method to fabricate SPCs with precisely tailorable multi-scale structures, versatile surface morphology, and controllable optical properties, by combining droplet microfluidics with metal thin film deposition and thermal annealing. Three-tier SPCs have been constructed consisting of well-spaced AuNCs (3^{rd}-tier) anchored on well-ordered SiO_2NP nanopatterns (2^{nd}-tier) confined in microspherical templates (1^{st}-tier). The 2D array of AuNCs (3^{rd}-tier) is distributed evenly on each SiO_2NP (2^{nd}-tier) with exquisite control over size, number density and topography. These SPCs possess both PSB and SPR resonances, which can be controlled by varying the structural dimensions at different length scales and the constituent materials of the 2^{nd}-tier and 3^{rd}-tier for on-demand applications. These three-tier SPCs can be transferred to or encapsulated in flexible materials to obtain a designed colorful pattern for anti-counterfeiting, which is caused by the structure-enhanced optical properties.

2. Results and discussion

2.1. Fabrication of three-tier SPCs

The process for fabrication of three-tier SPCs, combining droplet microfluidics with metal thin film deposition and metal dewetting processes, is shown in **Figure 1**. Details of the fabrication process are described in the Methods section. The droplet microfluidics platform is excellently suited for the production of well-ordered hexagonal two-tier SPCs with high uniformity and controllability, as it produces monodisperse microdroplets that encapsulate metered amounts of SiO_2NPs, and provide excellent spherical templates for the confinement-induced assembly of the SiO_2NPs.

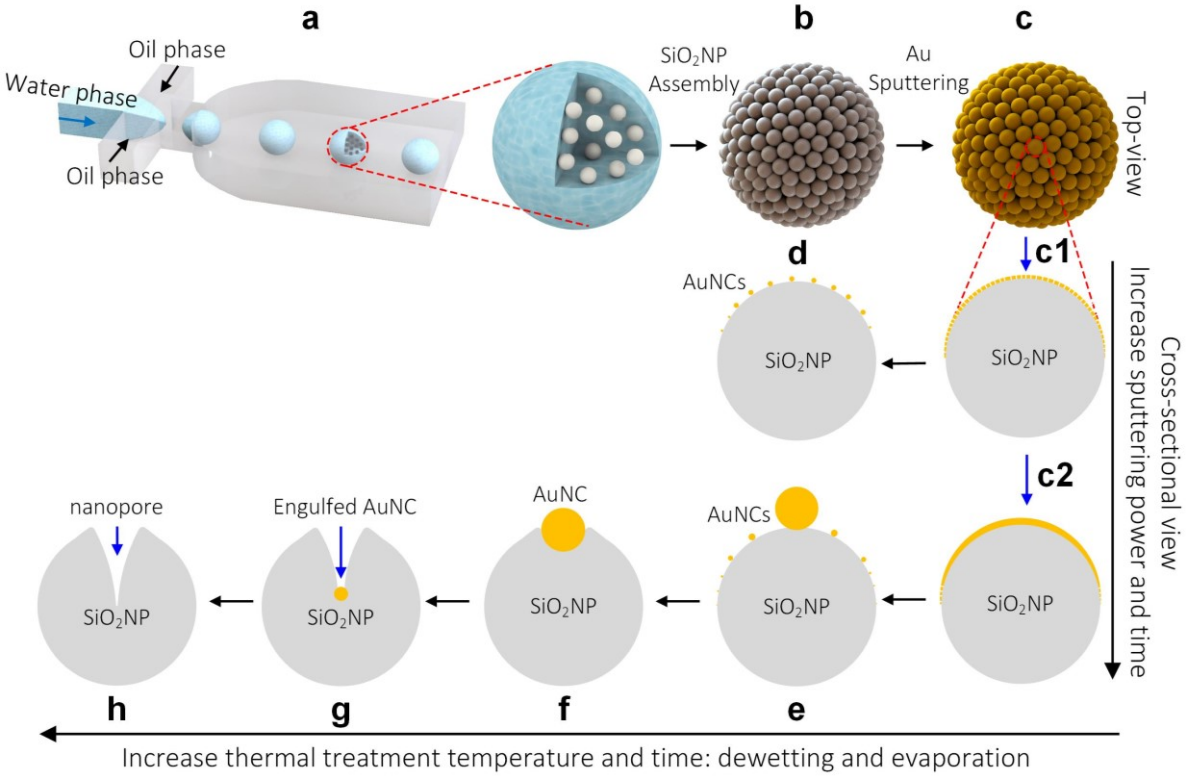

Figure 1. Schematic diagram of SPC fabrication process, combining droplet microfluidics with metal film deposition and thermal annealing. (**a**) Microdroplet generation via a droplet generator. (**b**) A two-tier SPC is formed *via* evaporation induced assembly of SiO_2NPs, featuring well-ordered nanopatterns. (**c**) Au-coated two-tier SPCs are obtained by sputtering Au films on the as-prepared two-tier SPCs with different thicknesses, showing initially discontinuous Au films (**c1**) and subsequently continuous Au films (**c2**) distributed on SiO_2NPs. Thermal annealing the Au-coated two-tier SPCs yields three-tier SPCs with various

surface morphologies including (**d**) multiple small AuNCs distributed uniformly on each SiO_2NP, (**e**) one large AuNC anchored on each SiO_2NP and small AuNCs encircled at the rim of SiO_2NPs, (**f**) one large AuNC anchored on each SiO_2NP, (**g**) one AuNC engulfed into each SiO_2NP, and (**h**) one closed-end nanopore formed in each SiO_2NP.

2.2. Manipulating the 3rd-tier morphology of the SPCs

By controlling the parameters (power and duration) of Au film deposition and thermal annealing process (temperature and duration), a variety of hierarchical structures of SPCs can be obtained, as summarized in **Figure 1**. In order to clearly label the parameters for the obtained SPCs, the nomenclature of $Au_{n\,s}^{m\,W}T_{y\,h}^{x\,°C}$@SPC is used, in which, *m* and *n* describe the sputtering parameters of power and duration, respectively, *x* and *y* are the used thermal annealing temperature and duration, respectively. For instance, $Au_{5s}^{100W}T_{1h}^{800°C}$ @SPC represents a SPC prepared by sputtering an Au film at 100 W for 5 s, and annealing at 800 °C for 1 h.

The morphology of a sputter-deposited Au film on a nanostructured surface with periodically arranged nanoparticles significantly differs from that on a flat surface, as shown in **Figure S1** in the Supporting Information (SI). On the flat surface, the sputtered Au film is distributed evenly over the entire surface, gradually forming a continuous film with increasing sputtering power and duration. However, on the nanostructured surface, individual nanofilms form on each nanoparticle surface. At high temperature, the solid Au film can dewet into isolated nanocrystals driven by the surface capillary flow.[53] The part of the nanofilm on the top of the nanoparticle thereby behaves differently from the part along the rim of the nanoparticle. Various 3rd-tier morphologies of AuNC arrays on SPCs can be obtained by high temperature annealing. **Figure 2a** shows an as-prepared two-tier SPC (Au_0@SPC) which features well-ordered nanopatterns of 300 nm SiO_2NPs as the 2nd-tier. To

optimize the shape and crystallinity of the formed 3rd-tier AuNCs on the 2nd-tier SiO_2 nanopatterns, we investigated the effect of the annealing temperature (**Figure S2**). We found that AuNCs with high crystallinity and regular disk (shape) were obtained by annealing at 800 °C for 1 h in ambient environment. Therefore, in the following section, Au-coated SPCs are studied that were treated at 800 °C for 1 h.

When sputtering a thin Au film (for example, at 100 W for 5s, Au_{5s}^{100W}@SPC, **Figure 2b**) onto the as-prepared two-tier SPC (Au_0@SPC), discontinuous Au films with small grain size were obtained. By a subsequent annealing process at 800 °C for 1 h ($Au_{5s}^{100W}T_{1h}^{800°C}$@SPC, **Figure 2c**) in air without flow, this discontinuous Au film dewetted in multiple small AuNCs (3rd-tier), with approximately the same number density on each SiO_2NP. The grain size of the discontinuous Au film can be increased by precise control over the sputtering parameters (for instance, at 200 W for 5 s, Au_{5s}^{200W}@SPC, **Figures 2d** and **S3**), after which the same annealing program resulted in relatively large AuNCs, distributed on each SiO_2NP ($Au_{5s}^{200W}T_{1h}^{800°C}$@SPC, **Figure 2e**). On a further increase in Au film thickness, more than one patch of continuous Au film covered the top surface and a discontinuous film was obtained along the rim of each SiO_2NP (Au_{10s}^{200W}@SPC, **Figure 2f**). On dewetting this resulted in the formation of multiple AuNCs with a random size distribution confined on top of each SiO_2NP ($Au_{10s}^{200W}T_{1h}^{800°C}$@SPC, **Figure 2g**). Further increasing the Au film thickness (sputtering at 200 W for 15 s and 20 s) led to the formation of only a single thick continuous Au film on the top surface of each SiO_2NP (red circles in **Figure 2h** and **2j**), whereas the Au films at the rim of each SiO_2NP remained discontinuous (blue arrows in **Figure 2h** and **2j**). Dewetting of the continuous Au film resulted in a single large AuNC anchored on top of the SiO_2NP, while dewetting of the discontinuous Au film along the rim resulted in multiple small AuNCs (for example, $Au_{15s}^{200W}T_{1h}^{800°C}$@SPC, **Figure 2i** and $Au_{20s}^{200W}T_{1h}^{800°C}$@SPC**, Figure 2k**).[53,54]

The Au film completely covered each SiO_2NP when further increasing the sputtering duration (**Figures S4a-c**), which resulted in the formation of one large AuNC of irregular shape and inhomogeneous size covering more than one SiO_2NP after the thermal dewetting (**Figures S4d-f**). We expect that the formation process in this case is driven by favorable surface energy change when the Au detaches from the void-Au interface.[53] From the above we concluded that the number density and size of AuNCs on each SiO_2NP unit can be well controlled by tailoring the deposited Au film morphology in a straightforward and robust manner, with the potential to apply in surface-enhanced Raman spectroscopy according to the 2D AuNC lattice on the PC structure.[55]

The size and distribution of the obtained well-spaced AuNCs on the SiO_2 nanopattern thus depends on both the Au film thickness and the size of the SiO_2NPs. **Figure S5a** shows the diameter of AuNCs on top of each SiO_2NP as determined from HR-SEM images. A clear increase is observed with sputtering power and duration, especially for the large AuNCs which contain most of the mass of the deposited Au. The edge-to-edge distance between two adjacent large AuNCs was also measured from the HR-SEM images as shown in **Figure S5b**. We have furthermore investigated the influence of the SiO_2NP diameter on the diameter and edge-to-edge distance of obtained AuNCs (**Figures S5c** and **5d**). An increase in the SiO_2NP diameter enlarged the deposited Au film area, especially the continuous Au film area on top of SiO_2NP. As a result, under the same thermal annealing conditions, larger AuNCs were obtained (**Figures S5c** and **S6**).

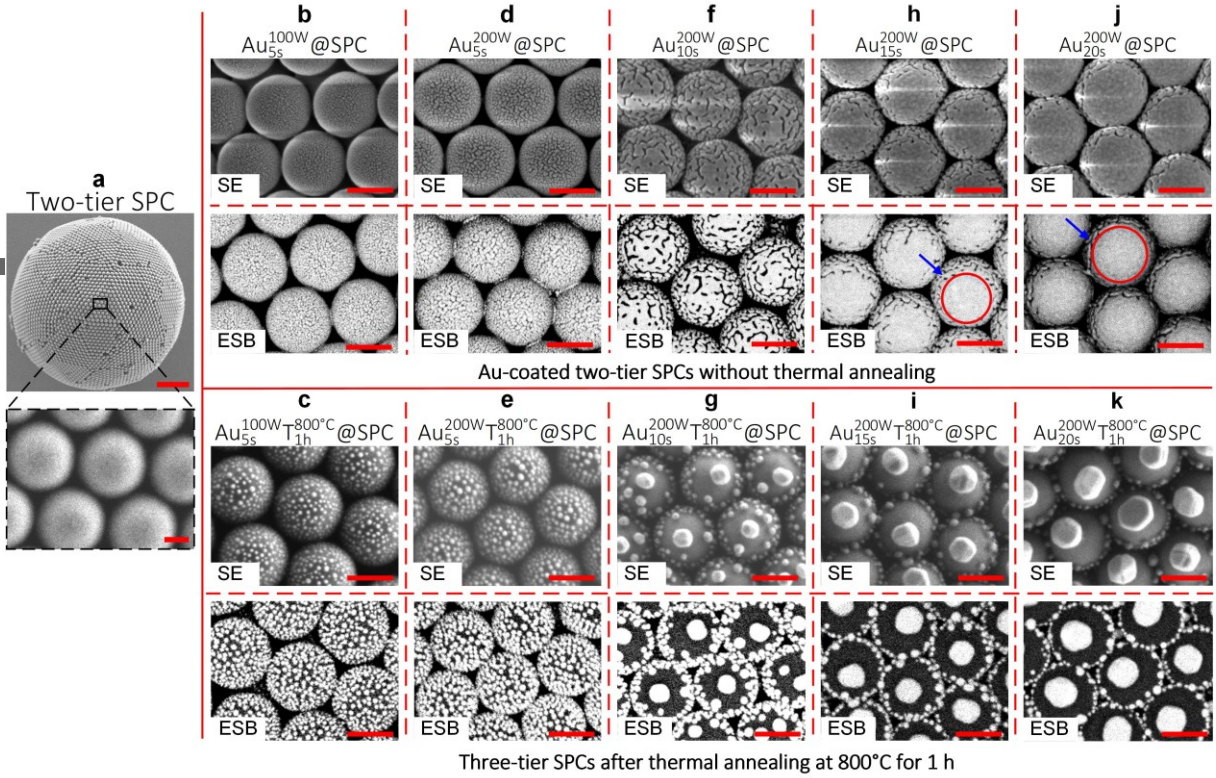

Figure 2. Au film thickness-controlled surface morphology of fabricated SPCs. Top-view high resolution scanning electron microscopy (HR-SEM) images of surface morphologies of various hierarchical SPCs. (**a**) A two-tier SPC (scale bar: 2 μm) assembled from SiO_2NPs (300 nm in diameter), and an enlarged image showing the surface morphology of a single SPC (scale bar: 200 nm). (**b**-**k**) HR-SEM images (scale bar: 200 nm) of surface morphology of corresponding SPCs with Au films and well-spaced AuNC arrays before and after thermal dewetting. Au films prepared by sputtering at (**b**, **c**) 100 W for 5 s, (**d**, **e**) 200 W for 5 s, (**f**, **g**) 200 W for 10 s, (**h**, **i**) 200 W for 15 s, and (**j**, **k**) 200 W for 20 s, respectively. The HR-SEM images were taken using the secondary electron (SE) detector, and the electron selective backscattered (ESB) detector – white color indicates the Au covered areas. The red circles indicate the areas coated with a continuous Au layer. Top-view HR-SEM images (scale bar: 200 nm) of the three-tier SPCs with different surface morphology after dewetting (**c**, **e**, **g**, **i**, **k**), corresponding to the Au-coated two-tier SPCs in (**b**, **d**, **f**, **h**, **j**), respectively.

As the annealing temperature can affect the Au mass transport, further experiments were performed to explore the morphology of AuNC arrays by controlling the annealing programs while keeping the Au film thickness fixed at 200 W for 15 s. **Figure 3** shows the schematic diagrams (cross-sectional view of the outer layer) and top-view HR-SEM images of the obtained three-tier SPCs with different surface morphologies. **Figure 3a** shows the surface morphology of an Au-coated two-tier SPC (Au_{15s}^{200W}@SPC) consisting of SiO_2NPs 300 nm in diameter. As discussed above, annealing Au_{15s}^{200W}@SPC at 800 °C for 1 h resulted in a single large AuNC anchored on top of each SiO_2NP surface and multiple small AuNCs at the rim of the SiO_2NP (indicated by the red arrow in the top-view close-up HR-SEM image in **Figure 3b** and the side-view HR-SEM image in **Figure S7a** for $Au_{15s}^{200W}T_{1h}^{800°C}$@SPC). In this experiment, air flow was employed to increase the Au mass transport from the tube furnace chamber to the outlet and a temperature of 1000 °C was chosen (close to the melting temperature of Au of 1064 °C).[56] Annealing the Au_{15s}^{200W}@SPCs at 1000 °C for 10 h with an air flow rate of 250 $L \cdot h^{-1}$ resulted in complete evaporation of small AuNCs at the rims, thus leaving only one AuNC (diameter 122±4 nm) on each SiO_2NP ($Au_{15s}^{200W}T_{10h}^{1000°C}$@SPCs, as shown in **Figures 3c** and **S7b** for the close-up side-view HR-SEM images, respectively). The resulting 3rd-tier AuNC arrays showed a hexagonal lattice, corresponding to the 2nd-tier SiO_2NP nanopatterns, which shows potential applications in diagnostics when functionalizing the AuNCs.[40] For example, secondary AuNCs can bind to the AuNC arrays of the 3rd-tier via biomolecules, resulting in a color change or spectral shift for biodetection with high sensitivity.[57] Further increasing the annealing duration to 20 h at 1000 °C induced a significant decrease in the size of the AuNCs (diameter 51±5 nm). Meanwhile, AuNCs started to be engulfed into the SiO_2NPs ($Au_{15s}^{200W}T_{20h}^{1000°C}$@SPCs, the close-up top-view HR-SEM image in **Figure 3d**), accompanied by the formation of silica ridges (indicated by the red arrows in **Figures 3d** and **3e**). This phenomenon has been previously described and

analysed by our group.[56] The engulfment of AuNCs into the SiO_2NPs with a certain depth can be explained by the Au-evaporation induced mass transport due to capillary forces.[56,58] When annealing at 1000 °C for 30 h, the AuNCs penetrated deeper into the SiO_2NPs until they completely evaporated ($Au_{15s}^{200W}T_{30h}^{1000°C}$@SPCs), leaving closed-end nanopores (entrance diameter 47±3 nm) connected to the SiO_2NP surface (**Figure 3e**). The cross-sectional HR-SEM images in **Figure S7c** confirms the engulfment of AuNCs into SiO_2NPs (indicated by the red arrow) and the existence of closed-end nanopores (indicated by the yellow arrow). As a result, an over thermal annealing process can result in complete evaporation of AuNCs in the nanopores. In this way, the size and depth of the formed nanopores was determined by the initial size of the formed AuNCs and the evaporation rate.[56]

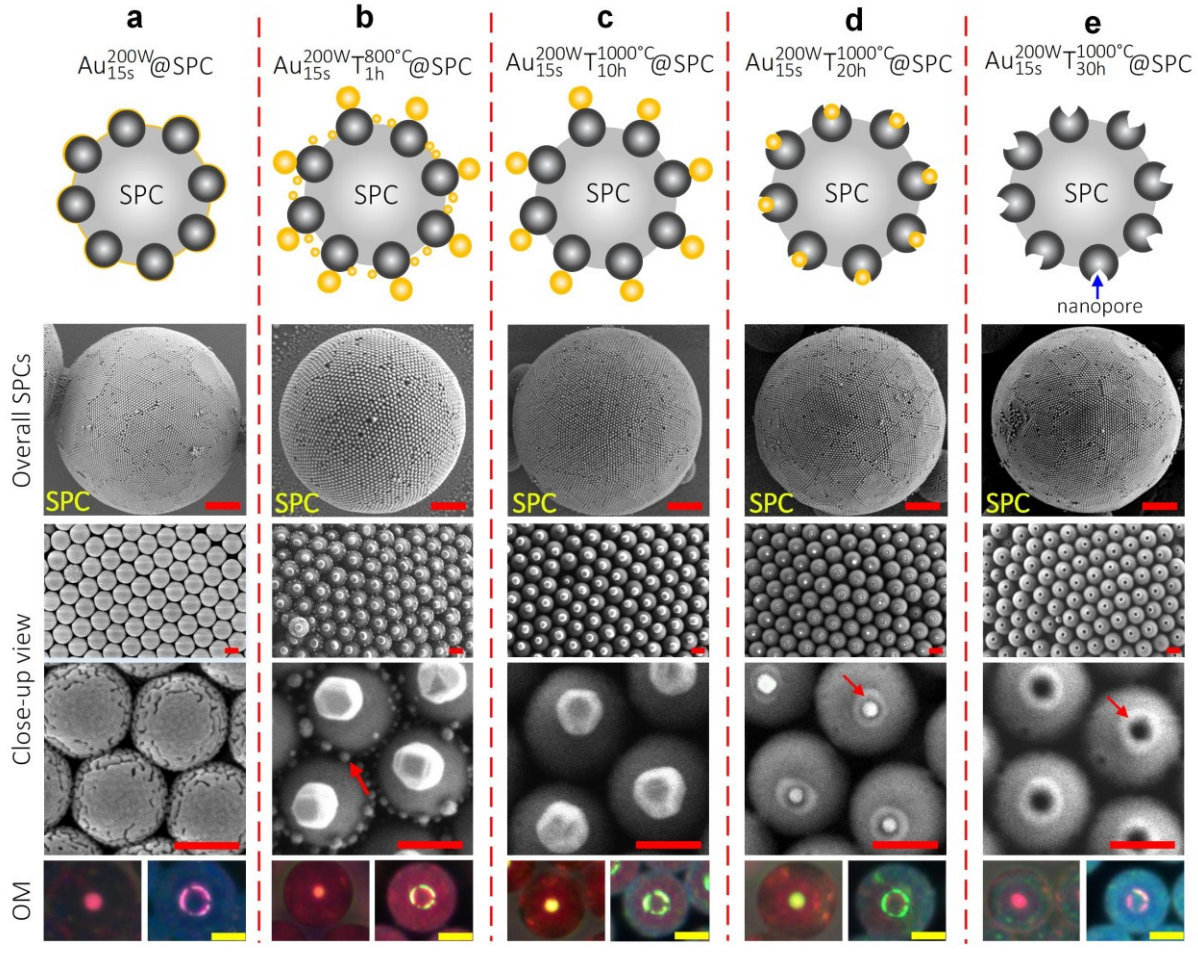

Figure 3. Thermal annealing program controlled surface morphology of fabricated SPCs. Diagrams of fabricated SPCs with various surface morphology, and their corresponding HR-SEM images for overall top-view SPCs (scale bar: 2 μm) and close-up details (scale bar: 200 nm), as well as optical microscopy images (OM, scale bar: 10 μm) under bright-field (left) and dark-field (right) illumination modes. (**a**) An Au-coated two-tier SPC (Au_{15s}^{200W}@SPC). (**b**-**e**) Three-tier SPCs with different surface morphologies fabricated by annealing the Au_{15s}^{200W}@SPC under different thermal treatment parameters at (**b**) 800 °C for 1 h without air flow, 1000 °C with an air flow rate of 250 $L \cdot h^{-1}$ for (**c**) 10 h, (**d**) 20 h and (**e**) for 30 h.

By controlling the Au film dewetting and evaporation on the as-prepared two-tier SPCs via the thermal treatment parameters, well-spaced AuNCs can be manufactured with high reproducibility in size, gap distance and geometric pattern. In comparison to the dewetting of Au films on flat surfaces (**Figure S8**),[59] and other approaches for fabrication of AuNC arrays such as physicochemical assembly,[60] a specific morphology of deposited Au films is obtained, leading to well-spaced 3rd-tier AuNC nanoarrays with controllable density and patterns. These hierarchical SPCs evince various structural colors, as shown in **Figure 3** (OM images in the last row), with high potential for application in anticounterfeiting and sensing.[61] Although patterning of plasmonic materials with well-spaced arrays on a flat surface were also studied by electron beam lithography for displays in which the color was raised from SPR properties,[62] it required expensive equipment and was time-consuming. Moreover, the patterned plasmonic arrays on the hard substrate was fixed, which was not flexible and also difficult to transfer to other substrate materials, for example, a flexible polymer film.

We furthermore investigated the possibility of manufacturing the three-tier SPCs using different materials. A layer of TiO_2 film was coated on the initial two-tier SPCs as an

alternative 2nd-tier surface material before depositing Au film. We then successfully prepared three-tier SPCs with TiO_2-coated SiO_2NPs (**Figure S9**). Platinum (Pt) was also deposited onto the two-tier SPCs as the 3rd-tier material instead of Au to obtain three-tier SPCs featuring PtNC arrays (**Figure S10**). These results prove that our approach is applicable to various material combinations, enabling on-demand preparation of SPCs with designed physical and chemical properties for a variety of applications, such as catalysis, light harvesting, and diagnostics.

2.3. Optical properties of fabricated hierarchical SPCs

Figure 4 shows OM images of freshly prepared two-tier and three-tier SPCs consisting of SiO_2NPs with different sizes, and their corresponding reflection spectra under BF and DF illumination modes, respectively. We have to note that the reflection percentage of *y* axis in spectra is the observed intensity of the measured samples under BF and DF illumination modes, and in both cases, a flat silicon wafer was used as a 100 % reflection under BF mode (the details of optical measurements are described in Methods section).

The Au films were prepared using the same parameters as in **Figure 2**, with all Au-coated SPC samples being annealed at 800 °C for 1 h. It was found that the structural color of fresh two-tier SPCs changed from green to orange and red when the SiO_2NP diameter (*D*) increased from 220 nm to 250 nm and 280 nm, under the BF (indicated by "No Au" in **Figures 4a**, **c** and **e**, and **Figure S11a** in the SI). For exploring the scattering of the AuNC arrays, the spectra of these fresh two-tier SPCs were also recorded under DF, showing a red shift with increasing SiO_2NP diameter (indicated by "No Au" in **Figures 4b**, **d**, **f**, and **S11b**). We thereby found that the deviation of the measured reflected peaks between the BF and DF mode (**Figures S11a** and **b**) can be attributed to the angle difference of the light incident on

the sample between the BF and DF modes. The white light paths under the used BF and DF illumination modes are schematized in **Figure S12**.

The structural color changes in both (BF and DF) modes can be attributed to a variation of the lattice spacing of the PC structures.[23] An increase in the size of the SiO_2NPs gives rise to a red shift in the reflection spectra of the fresh two-tier SPCs, as observed in both BF and DF modes. Note that, annealing the fresh two-tier SPCs at 800 °C for 1 h (the same annealing condition as in **Figure 2**), the Bragg diffraction of these annealed two-tier SPCs showed a blue shift compared to the fresh two-tier SPCs (**Figure S13**). This can be attributed to the narrowing of the lattice spacing after high temperature annealing. The measured Bragg diffraction peaks of these annealed two-tier SPCs increased from 476 nm to 562 nm and 586 nm (indicated in the reflection spectra of **Figure S13**) with increasing SiO_2NP diameter, which is relatively consistent with the calculated values of 488 nm, 555 nm, and 621 nm with a standard deviation (SD) of 2.45%, 1.25%, and 5.64%, respectively, using the estimated Bragg-Snell equation:[63]

$$\lambda = 2\sqrt{\frac{2}{3}} D \sqrt{n_{eff}^2 - (\sin\theta)^2} \cdot$$

Here D is the diameter of the SiO_2NP, n_{eff} is the average refractive index of the building block material, and θ is the angle of incidence of light with respect to the normal (under BF mode, assumed $\theta = 0°$). The annealed two-tier SPCs containing the volumes of silica and air in one microunit possess close to a hexagonally close-packed arrangement. For a hexagonally close-packed assembly corresponding to [111] plane of the face-centered cubic lattice, the volume fraction of the silica is approximately 0.74 with a void fraction of 0.26 confined in a single SPC.[64] We think that the slight deviation between the measured and the estimated Bragg diffraction peaks is mainly caused by a small amount of disorder in the periodic lattices, resulting in a change of the volume fraction of silica and air in one microunit. This can be confirmed by the Bragg diffraction peak intensity in **Figure S13**, since the intensity of the

Bragg diffraction peak indicates the crystalline order confined in the periodic PC structures.[33]

Compared to the fresh two-tier SPCs, three-tier SPCs showed both PSB and SPR optical properties (**Figure 4**), which are characterized by the BF and DF illumination modes, respectively. These three-tier SPCs were composed of SiO_2NPs with diameters of 220 nm (**Figures 4a** and **b**), 250 nm (**Figures 4c** and **d**), and 280 nm (**Figures 4e** and **f**). When AuNCs were introduced, making the SPCs from a fresh two-tier structure to a three-tier structure, the Bragg diffraction peak showed a blue shift in both the OM images and the corresponding reflection spectra (**Figures 4a**, **c** and **e**) under BF mode. We attribute this mainly to the narrowing of the lattice spacing during the thermal annealing treatment. However, the Bragg diffraction peaks of three-tier SPCs do not show a significant change (indicated by the red dotted line in **Figures 4a**, **c** and **e**), when varying the 3rd-tier AuNC arrays starting from the multiple small AuNCs on each SiO_2NP ($Au_{5s}^{100W}T_{1h}^{800°C}$) to the hexagonal patterns comprising one large AuNC on top of each SiO_2NP and smaller ones along the rim of each SiO_2NP ($Au_{20s}^{200W}T_{1h}^{800°C}$). Moreover, introducing the 3rd-tier AuNC arrays within the investigated range did not contribute significantly to n_{eff} (see detailed information in SI, the section of "Estimation of the n_{eff} of a three-tier SPC"), suggesting that the 3rd-tier AuNC arrays could not induce obvious change of Bragg diffraction peak.

The absorption peaks observed at approximately 520 nm wavelength under BF mode are attributed to the light absorption by the AuNCs. The absorption frequency is in agreement with literature reports.[40,65,66] This absorption gives the structural red color of these three-tier SPCs with varying surface morphology, as observed in the OM images and the spectra with enhanced reflection in the red spectral domain (**Figures 4a**, **c**, and **e**). Furthermore, we found that the PSB peaks and Au reflections of three-tier SPCs consisting of SiO_2NPs with diameters of 250 nm and 280 nm overlapped in the red spectral region (blue to red curves in

Figures 4c and **e**). This suggests that the 3rd-tier AuNC arrays cannot influence the Bragg diffraction of the periodic structures, but that a synergistic effect of both PSB and Au reflection can be achieved by tailoring the Bragg diffraction.

Under the DF mode, reflection peaks caused either by Bragg diffraction of the PC structures or by Au scattering of the AuNC arrays were observed (indicated in **Figures 4b**, **d** and **f**). We found that when the PSB (in blue spectral region) was located separately from the Au scattering (in red spectral region) (**Figure 4b**), the PSB is not influenced by the surface morphology of 3rd-tier AuNC arrays. The scattering plateau (from cyan to red curves in **Figure 4b**) or peaks (from cyan to red curves in **Figures 4d** and **f**) in the red spectral region result from the AuNC arrays. On excitation by incident light of the AuNCs, surface plasmon oscillations are damped non-radiatively by absorption due to the electron-photon interactions, and/or radiatively by resonant scattering[67] For small AuNCs, only plasmon absorption occurs, whereas both absorption and scattering occur simultaneously on large AuNCs (larger than ~50 nm in diameter)[68] This is shown in **Figure 4b** (blue to red curves indicated by "Au scattering") for increasing AuNC size. No sharp scattering peak was observed in **Figure 4b**, which is attributed to the mismatch between the PSB of the periodic lattices (indicated by "PSB") and the Au scattering peak (indicated by "Au scattering"). However, **Figures 4d** and **f** do show an overlap of the PSB and Au scattering peaks at the red spectral region. The red shift of these overlapping peaks is caused by an increase in the AuNC diameter (**Figure S14**). A red shift of PSB peak can lead to an increase in intensity of this overlapping peak (for example, red curves in **Figures 4d** and **f**). We found that the PSB located in the red spectral region can enhance the scattering of AuNC arrays (**Figures 4d** and **f**). This suggests that the AuNC array scattering can be amplified by the PC structure due to the multiple and repeated light scattering confined in PC structures, when both are located in the same spectral region.

Furthermore, the optical properties were investigated of SPCs with 3rd-tier AuNC arrays with one large AuNC on top and multiple small ones along the rim of each SiO_2NP, as well as those with a single large AuNC on top of each SiO_2NP creating a well-spaced hexagonal lattice. Characterization was performed in ambient air (**Figure S15**) and homogenous environment (SPCs immersed in hexadecane with a reflective index of 1.43, **Figure S16**), respectively. We found a blue shift of SPCs from a structure with one large AuNC on top and multiple small ones along the rim of each SiO_2NP to a structure with only a single large AuNC on top, when the PSB and Au reflection/scattering overlap in the red spectra region. Possibly, we attribute this to the synergistic effects of PSB and Au reflection, as well as a decrease in the AuNC size and an increase in the AuNC interparticle distance[69] caused by the Au evaporation during the thermal annealing process. Again, we found an obvious red shift with increasing intensity of this overlap peak (**Figures S15d** and **f**), and we attribute this to the increased size of the formed AuNCs on the corresponded PC structures and a red-shifting of the PSB peak. In summary, these fabricated three-tier SPCs show not only PSB (Bragg diffraction) properties resulting from the periodic arrangements in the underlying 2nd-tier patterns, but can also exhibit SPR effects (absorption and plasmonic scattering) due to the AuNC arrays anchored on 2nd-tier of SiO_2NP patterns. The key finding is that both the PSB and SPR resonances in this hybrid hierarchical SPCs can be precisely controlled by the size of SiO_2NPs and the surface morphology of the 3rd-tier AuNCs to achieve the synergistic effects.

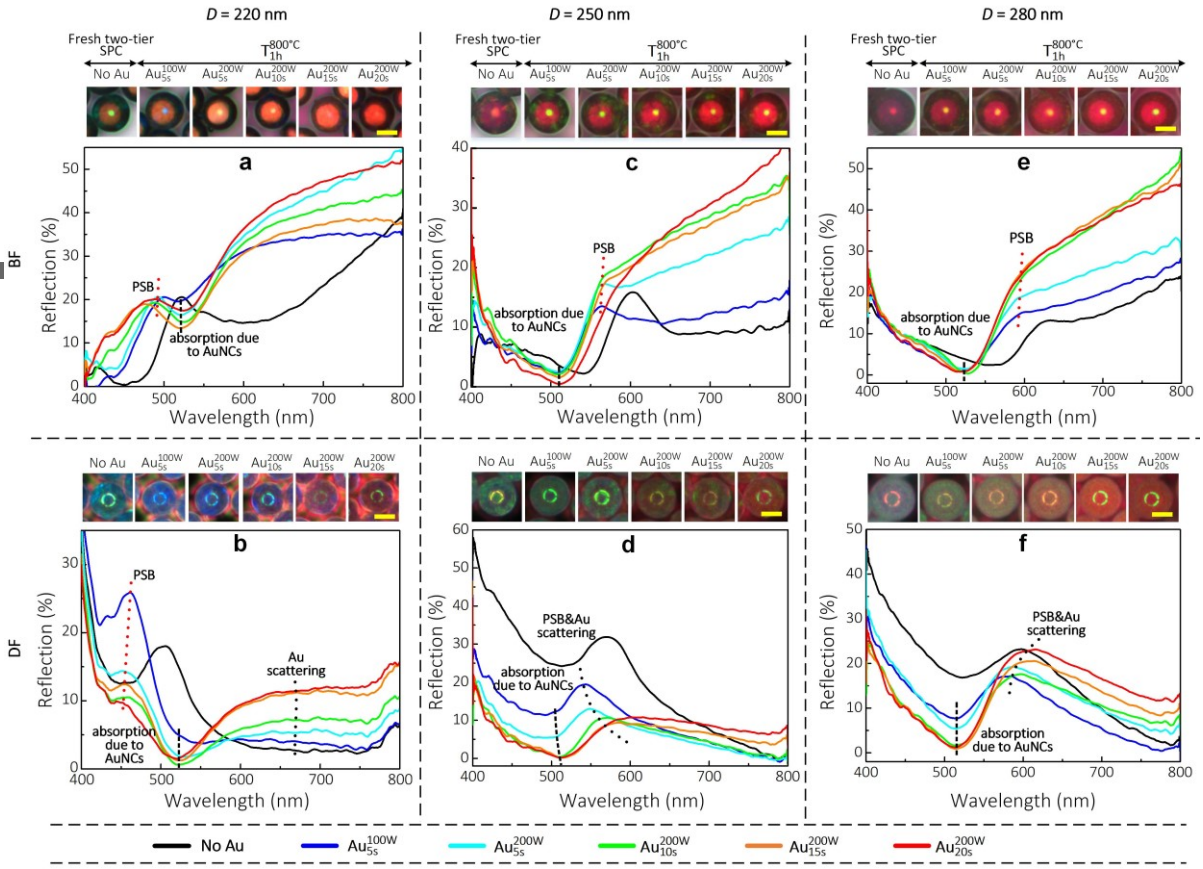

Figure 4. Optical properties of SPCs controlled by Au film thickness. BF and DF images (scale bar: 10 μm) of prepared fresh two-tier and three-tier SPCs consisting of SiO_2NPs with diameters of (**a**, **b**) 220 nm, (**c**, **d**) 250 nm, and (**e**, **f**) 280 nm, and their corresponding reflection spectra obtained in (**a**, **c**, **e**) BF and (**b**, **d**, **f**) DF. The red dotted line indicates the PSB of PC structures, the black dashed line indicates the absorption due to AuNCs and the black dotted line indicates the Au scattering or overlapping peak of Au scattering and PSB. The three-tier SPCs were fabricated by sputtering Au films at 100 W for 5s, 200 W for 5, 10, 15, and 20 s, on as-prepared fresh two-tier SPCs, followed by thermal annealing at 800 °C for 1 h in air without flow.

2.4. Demonstration of three-tier SPCs for anticounterfeiting

We employed these hierarchical SPCs to fabricate flexible anticounterfeiting films, showing different structural colors (**Figure 5**). **Figure 5a** presents the fabrication process (see

details in the Methods section) of the flexible films with the "MESA+" logo, showing diverse structural colors. The close-packed monolayers of two-tier SPCs containing SiO_2NPs with different diameters are shown in **Figure S17**. The photographs of the obtained flexible films with 'MESA+' logos were captured using a smartphone camera (iPhone 6s, A1700) with and without a flash (**Figure 5b**). A patterned monolayer of hierarchical SPCs was embedded into a flexible film (cured poly(dimethylsiloxane) (PDMS)). A transparent area is obtained by the assembled two-tier SPCs as the refractive indices of PDMS (n = 1.4) and SiO_2NPs (n = 1.45) are matched, while the "MESA+" logo with diverse structural colors resulted from the AuNC array scattering of the three-tier SPCs. Without a flash, three-tier SPCs showed similar orange-red structural colors with a low contrast, though they consisted of SiO_2NPs with different diameters. This agrees with the OM images and the corresponding reflection spectra (**Figure 5c**) under the BF mode. The spectra of the "MESA+" logo collected under the BF showed the absorption of AuNCs approximately at 550 nm wavelength and the strong reflection of AuNCs in the red spectral region, which explains the structural colors of these "MESA+" logo stamps that are similar to those captured under the BF mode (inset of **Figure 5c**) and using the phone camera without a flash. When using a flash, these flexible films showed diverse structural colors with color saturation increasing with SiO_2NP size. The reflection spectra and corresponding OM images (**Figure 5d**) show the structural color of the "MESA+" logo, caused by the synergistic effect of the Au scattering and the PSB. We found that the scattering peak show a red shift and an increase in intensity with increasing SiO_2NP diameter, since the diameter of corresponded AuNCs on the SiO_2NP nanopatterns are increased. We attribute this again to the Au scattering enhancement caused by the PC structure, as explained in **Figures 4d** and **f**. Therefore, such flexible films embedded with different types of hierarchical SPCs can be applied as anticounterfeiting stamps and in the field of security according to the remarkable contrast difference of structural colors when

captured with and without a flash by the mobile phone camera. **Video S1** (SI) demonstrates the flexibility of the obtained film. Moreover, due to the high symmetric geometry of the two-tier SPCs and the formed AuNCs (**Figure S7a**), these flexible films exhibits angle-independent structural color (**Figure S18**). In addition, the flexible films manufactured by this strategy can benefit from its high mechanical and chemical stability, excellent scratch resistance and low photodegradation.[62,70]

Using the same fabrication method, the "MESA+" logo, which composed of randomly distributed AuNCs of inhomogenous size and shape (**Figure S19a**), was created on a flat silicon (Si) substrate by Au film sputtering and dewetting and transferred to a flexible film (**Figure S19**). This "MESA+" logo is hard to discern on the flexible film (indicated by the dashed orange line in **Figure S19b**), since the AuNCs formed directly on the Si substrate cannot be transferred to a flexible film because of their strong adhesion to the Si surface. Additionally, the structural color of "MESA+" logo on Si substrate captured with a flash is much weaker than the ones on the SPC structures, as demonstrated by the reflection spectra (**Figure S19c**). Under the DF mode, a broad scattering peak at approximately 640 nm was observed, a 10 times longer integration time than with the other specimens. In addition, the patterns of "SCNU" letters filled with various types of SPCs showed a variety of structural colors when exposed to media with different dielectric constants (**Figure S20**). The structural colors are much more easily identified under the DF than BF mode, due to the enhanced scattering under DF; as a result, this obvious contrast could be used for information encryption in various fields.

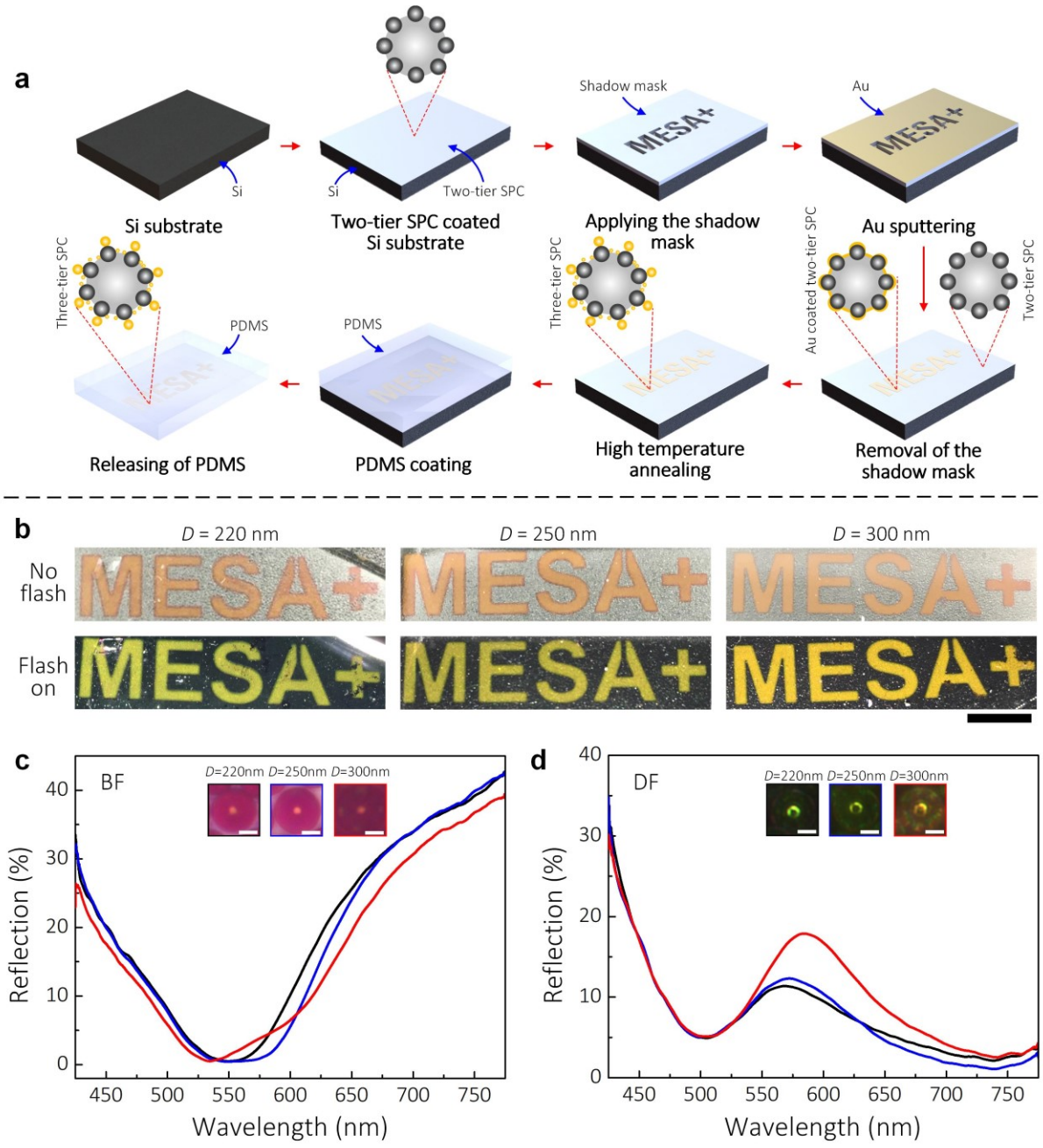

Figure 5. Manufacturing of flexible anticounterfeiting stamps using the fabricated hierarchical SPCs. (**a**) Fabrication process of flexible film with "MESA+" logo. (**b**) Photographs (scale bar: 5 mm) of the fabricated flexible films with "MESA+" logo showing different structural colors, which were embedded with two-tier and three-tier SPCs of $Au_{15s}^{200W}T_{1h}^{800°C}$@SPCs consisting of SiO_2NP with different diameters, and captured using a smart phone with and without a flash. OM images (scale bar: 10 μm) and reflection spectra were obtained under the BF (**c**) and DF (**d**) modes.

3. Conclusion

In summary, multitier SPCs with tailorable architectures and controllable optical properties of both the PSB and SPR have been achieved by a robust and facile method combining droplet microfluidics with metal film deposition and programmed thermal annealing. Two-tier SPCs were created by confined assembly of SiO_2NPs in microdroplets produced by using a microfluidic chip. The 3rd-tier morphology of the AuNC arrays on the SiO_2NP nanopatterns was produced by the dewetting and evaporation of Au films during a thermal annealing process. In this way, three levels of hierarchical structure can be integrated by (i) using microfluidics to create the 1st-tier micrometer-size spheres, (ii) nanoparticle assembly for defining the 2nd-tier nanopatterns, and (iii) deposited metal film dewetting and evaporation for generating the 3rd-tier AuNC arrays with high controllability and stable reproducibility. As a result, the structure-enhanced optical properties of both PSB and SPR can be well controlled, creating enhanced functionalities of the hierarchical SPCs. We have demonstrated the potential applications of the fabricated three-tier SPCs for anticounterfeiting and information security. The designed pattern consisting of these produced hierarchical SPCs can be easily identified using the mobile phone with a flash due to the created high contrast instead of the low contrast captured without a flash. The SPCs produced in this manner possess well-spaced arrays in both the 2nd-tier and 3rd-tier, providing a flexible platform to tailor the constituent materials of the 2nd-tier and 3rd-tier. These structures could be a high-potential platform in areas where arrayed structures (i) can be evolved into nanowires via the vapor-liquid-solid mechanism,[71] (ii) provide a point-of-care readout diagnostic device,[22] or are employed to create template-based assembly processes in nanospace.[72]

4. Methods

Materials. *N*-hexadecane (purity ≥ 99%) and sorbitan monooleate (Span 80) as a surfactant were both purchased from Sigma-Aldrich (the Netherlands). Silica building blocks with different diameters (200 ± 10 nm, 220 ± 10 nm, 250 ± 10 nm, 280 ± 10 nm, and 300 ± 10 nm) were provided by Nanjing Rainbow Company (Nanjing, China). The Au target (purity ≥ 99.999%) and Ti (purity ≥ 99.995%) target were both purchased from Kurt J. Lesker company.

Fabrication of two-tier SPCs. A flow-focusing poly(dimethylsiloxane) (PDMS) microfluidic chip was used to generate monodispersed droplets (**Figure 1a**). The fabrication of this flow-focusing PDMS microfluidic chip were reported elsewhere.[31] The oil phase (continuous phase) was *n*-hexadecane containing 20 wt% Span80. A SiO_2NP (300 mg·mL^{-1}) suspension was used as the water phase (dispersed phase). The water phase was sheared off into monodispersed droplets by the oil phase. The generated droplets served as templates encapsulating a certain amount of SiO_2NPs. Subsequently, these droplets were solidified by thermal evaporation in an oven at 60 °C overnight, yielding two-tier SPCs featuring well-ordered and close-packed hexagonal nanopatterns (**Figure 1b**). The Bragg diffraction wavelength of the two-tier SPCs can be tailored by varying the size of the used SiO_2NPs.

Thermal annealing of the Au-coated two-tier SPCs. A piece of silicon (Si) wafer treated with oxygen plasma (Femto Science Cute, Femoto Science Inc, Hwaseong-Si, Korea) was used as a support substrate for drop-casting the as-prepared two-tier SPCs dispersed in deionized (DI) water. A monolayer of assembled two-tier SPCs was obtained by passively drying at room temperature. Subsequently, a thin Au film was sputtered on the patterned two-tier SPCs (**Figure 1c**), using an ion-beam sputtering system (home-built T'COathy system, MESA+, the Netherlands). The morphology and thickness of the sputtered Au films can be varied by

controlling the sputtering power and duration. These Au-coated two-tier SPCs were then annealed in a tube furnace (Nabertherm, Nabertherm GmbH, Germany) at 800 °C (ramp-up temperature rate of 13.3°C min^{-1}) for 1 h, or at 1000°C (ramp-up temperature rate of 8.3°C min^{-1}) for 10 h, 20 h or 30 h with an air flow of 250 $L \cdot h^{-1}$, and subsequently cooled down passively to room temperature. As a result, three-tier SPCs featuring well-spaced AuNC nanoarrays on the as-prepared two-tier SPCs were fabricated with various morphologies of the 3rd-tier (**Figure 1d**).

Fabrication of flexible anticounterfeiting films. The as-prepared fresh two-tier SPCs were suspended in water and drop-casted onto a Si wafer to assemble into a monolayer. The Si wafer was treated with oxygen plasma to make the surface more hydrophilic in order to obtain a well-patterned monolayer of SPCs. Afterwards, the SPC suspension was drop-casted on it and left in air at room temperature for water evaporation. The microscale SPCs assembled on the Si surface during water evaporation to form a well-patterned monolayer arrangement (**Figure S17**). Subsequently, a shadow mask with "MESA+" logo was applied on the surface of the as-patterned two-tier SPCs on the Si wafer, followed by sputtering an Au film. As a result, only the area of "MESA+" was covered with the deposited Au film. Then this produced substrate was annealed at 800 °C for 1 h without air flow, resulting in different regions consisting of annealed two-tier SPCs and three-tier SPCs. Pouring a layer of liquid PDMS onto the surface of this substrate, baking it in an oven at 60 °C for 2 h, and peeling off the cured PDMS layer resulted in a flexible film with "MESA+" logo, showing different structural colors. Also, using the same fabrication method, the "MESA+" logo was directly fabricated on a piece of Si wafer surface. Followed by pouring a layer of liquid PDMS and curing process, the "MESA+" logo cannot be transferred onto the flexible film.

Optical characterization. The droplet generation was monitored and video-captured using an optical microscopy (Leica DMI 5000M, Wetzlar, Germany) equipped with a high-speed camera (High-speed camera photron, fastcam SA3, Model 60K-M1, Motion Engineering Company, Westfield, the United States). The reflection spectra of the produced two-tier/three-tier SPCs were recorded by using an optical microscopy (Leica DM 6000M, Wetzlar, Germany) under BF and DF illumination modes, respectively, matched with an optical spectrometer (Ocean optics HR4000, Ocean Optics Inc.), in ambient environment or in homogenous environment. The OM images and corresponding reflection spectra were all collected using 20 × (NA = 0.4) objective lens with a white light spot diameter of 1.1 mm. A flat silicon wafer was used as a reference with a 100% reflection under the BF mode, since the samples were on the silicon substrate. The silicon substrate fully covering a close-packed monolayer of produced hierarchical SPCs was used to collect the reflection spectra. The integration time was set at 100 ms, however, except that the case particularly was mentioned in the main text. The reflection spectra of obtained flexible films with "MESA+" logo supported by a piece of clean Si wafer were measured using the same method.

Scanning electronic microscopy characterization. The surface morphology of the produced two-tier/three-tier SPCs were characterized using a high-resolution scanning electronic microscopy (HR-SEM, GeminiSEM 500, Carl Zeiss Microscopy GmbH) with different detectors: secondary electron (SE), and electron selective backscattered (ESB). The electron backscattered signal was used to identify the SiO_2NPs and the Au film/ AuNCs based on their contrast difference. The sample for cross-sectional view was prepared by using a focused ion beam (FIB) system (FEI Nova 600 Nanolab FIB, United States).

Supporting Information

Supporting Information is available from the Wiley Online Library or from the author.

Acknowledgements

We appreciate the financial support from the National Key Research & Development Program of China (2016YFB0401502), the National Natural Science Foundation of China (No. 61574065), Guangdong Science and Technology Planning Project (No. 2016B090906004), Special Fund Project of Science and Technology Application (No. 2017B020240002), and the Guangdong Innovative and Entrepreneurial Team Program (2016ZT06C517); Pioneers in Healthcare voucher (project Ischemia on chip) of the University of Twente, MST and ZGT in the Netherlands; the Australian Research Council (Grant CE170100026); and the Oversea study of Guangzhou Elite Project support, China. The platforms of PCSIRT Project No. IRT_17R40, the National 111 Project, and the MOE International Laboratory for Optical Information Technologies are also appreciated for providing technical support. The authors thank Mark Smithers (NanoLab Cleanroom, University of Twente) for SEM analysis.

References

[1] F. Shao, J. Sun, L. Gao, S. Yang, J. Luo, *ACS Appl. Mater. Interfaces* **2011**, *3*, 2148.

[2] H. Xu, B. Yang, H. Li, G. Shi, N. Lu, D. Qi, W. Xu, L. Chi, *Langmuir* **2011**, *27*, 4963.

[3] D. Wang, A. Yang, A. J. Hryn, G. C. Schatz, T. W. Odom, *ACS Photonics* **2015**, *2*, 1789.

[4] Y. Li, C. Li, S. O. Cho, G. Duan, W. Cai, *Langmuir* **2007**, *23*, 9802.

[5] B. Su, Y. Tian, L. Jiang, *J. Am. Chem. Soc.* **2016**, *138*, 1727.

[6] W. K. Lee, C. J. Engel, M. D. Huntington, J. Hu, T. W. Odom, *Nano Lett.* **2015**, *15*, 5624.

[7] P. Kim, M. J. Kreder, J. Alvarenga, J. Aizenberg, *Nano Lett.* **2013**, *13*, 1793.

[8] H. E. Jeong, K. Y. Suh, J.-K. Lee, S. H. Moon, H. N. Kim, *Proc. Natl. Acad. Sci.* **2009**, *106*, 5639.

[9] Y. Sang, M. Li, J. Liu, Y. Yao, Z. Ding, L. Wang, L. Xiao, Q. Lu, X. Fu, D. L. Kaplan, *ACS Appl. Mater. Interfaces* **2018**, *10*, 9290.

[10] A. Tampieri, S. Sprio, A. Ruffini, G. Celotti, I. G. Lesci, N. Roveri, *J. Mater. Chem.* **2009**, *19*, 4973.

[11] Y. Zheng, H. Bai, Z. Huang, X. Tian, F. Q. Nie, Y. Zhao, J. Zhai, L. Jiang, *Nature* **2010**, *463*, 640.

[12] D. Whang, S. Jin, Y. Wu, C. M. Lieber, *Nano Lett.* **2003**, *3*, 1255.

[13] H. Lee, W. Manorotkul, J. Lee, J. Kwon, Y. D. Suh, D. Paeng, C. P. Grigoropoulos, S. Han, S. Hong, J. Yeo, S. H. Ko, *ACS Nano* **2017**, *11*, 12311.

[14] I. B. Burgess, M. Lončar, J. Aizenberg, *J. Mater. Chem. C* **2013**, *1*, 6075.

[15] P. Tan, Y. Liu, A. Zhu, W. Zeng, H. Cui, J. Pan, *ACS Sustain. Chem. Eng.* **2018**, *6*, 10385.

[16] J. D. Joannopoulos, P. R. Villeneuve, S. H. Fan, *Nature* **1997**, *386*, 143.

[17] E. Pavarini, L. C. Andreani, C. Soci, M. Galli, F. Marabelli, D. Comoretto, *Phys. Rev. B - Condens. Matter Mater. Phys.* **2005**, *72*, 045102.

[18] H. M. van Driel, W. L. Vos, *Phys. Rev. B - Condens. Matter Mater. Phys.* **2000**, *62*, 9872.

[19] M. S. Thijssen, R. Sprik, J. E. G. J. Wijnhoven, M. Megens, T. Narayanan, A. Lagendijk, W. L. Vos, *Phys. Rev. Lett.* **1999**, *83*, 2730.

[20] S. Tadepalli, J. M. Slocik, M. K. Gupta, R. R. Naik, S. Singamaneni, *Chem. Rev.* **2017**, *117*, 12705.

[21] Y. Lu, H. Yu, S. Chen, X. Quan, H. Zhao, *Environ. Sci. Technol.* **2012**, *46*, 1724.

[22] C. Fenzl, T. Hirsch, O. S. Wolfbeis, *Angew. Chem. Int. Ed.* **2014**, *53*, 3318.

[23] Y. Zhao, L. Shang, Y. Cheng, Z. Gu, *Acc. Chem. Res.* **2014**, *47*, 3632.

[24] Y. Zhao, Z. Xie, H. Gu, C. Zhu, Z. Gu, *Chem. Soc. Rev.* **2012**, *41*, 3297.

[25] M. SoljaČiĆ, J. D. Joannopoulos, *Nat. Mater.* **2004**, *3*, 211.

[26] G. von Freymann, J. I. L. Chen, V. Kitaev, G. A. Ozin, S. Y. Choi, *Adv. Mater.* **2006**, *18*, 1915.

[27] B. Yang, L. Xu, L. Jiang, X. Yan, X. Yao, J. Zhang, X. Gao, K. Zhang, *Adv. Mater.* **2007**, *19*, 2213.

[28] S. Takahashi, K. Suzuki, M. Okano, M. Imada, T. Nakamori, Y. Ota, K. Ishizaki, S. Noda, *Nat. Mater.* **2009**, *8*, 721.

[29] P. V. Braun, S. A. Rinne, F. García-Santamaría, *Adv. Mater.* **2006**, *18*, 2665.

[30] Z. Zhu, J. Liu, C. Liu, X. Wu, Q. Li, S. Chen, X. Zhao, D. A. Weitz, *Small* **2019**, *1903939*, 1.

[31] J. Wang, M. Jin, Y. Gong, H. Li, S. Wu, Z. Zhang, G. Zhou, L. Shui, J. C. T. Eijkel, A. Van Den Berg, *Lab Chip* **2017**, *17*, 1970.

[32] S. H. Kim, S. J. Jeon, G. R. Yi, C. J. Heo, J. H. Choi, S. M. Yang, *Adv. Mater.* **2008**, *20*, 1649.

[33] N. Vogel, S. Utech, G. T. England, T. Shirman, K. R. Phillips, N. Koay, I. B. Burgess, M. Kolle, D. A. Weitz, J. Aizenberg, *Proc. Natl. Acad. Sci. U. S. A.* **2015**, *112*, 10845.

[34] D. Liu, W. Cai, M. Marin, Y. Yin, Y. Li, *ChemNanoMat* **2019**, *11*, 1338.

[35] J. Feldmann, T. Zhang, P. C. Nickels, T. Liedl, J. Do, V. J. Schüller, R. Schreiber, E.-M. Roller, *Nat. Nanotechnol.* **2013**, *9*, 74.

[36] C. Hamon, S. Novikov, L. Scarabelli, L. Basabe-Desmonts, L. M. Liz-Marzán, *ACS Nano* **2014**, *8*, 10694.

[37] C. M. Soukoulis, M. Wegener, *Nat. Photonics* **2011**, *5*, 523.

[38] A. P. Alivisatos, T. Weiss, N. Liu, H. Giessen, M. Hentschel, *Science* **2011**, *332*, 1407.

[39] and M. V. Kreibig, Uwe, *Springer Sci. Bus. Media* **2013**, *25*, 13.

[40] S. Eustis, M. A. El-Sayed, *Chem. Soc. Rev.* **2006**, *35*, 209.

[41] K. A. Willets, R. P. Van Duyne, *Annu. Rev. Phys. Chem.* **2006**, *58*, 267.

[42] Y. Chen, K. Munechika, D. S. Ginger, *Nano Lett.* **2007**, *7*, 690.

[43] C. L. Haynes, C. R. Yonzon, X. Zhang, R. P. Van Duyne, *J. Raman Spectrosc.* **2005**, *36*, 471.

[44] Y. Li, C. Jing, L. Zhang, Y. T. Long, *Chem. Soc. Rev.* **2012**, *41*, 632.

[45] T. A. Klar, T. Franzl, J. Feldmann, A. Nichtl, G. Raschke, K. Kürzinger, S. Kowarik, C. Sönnichsen, *Nano Lett.* **2003**, *3*, 935.

[46] C. Novo, A. M. Funston, P. Mulvaney, *Nat. Nanotechnol.* **2008**, *3*, 598.

[47] X. Chen, H. Y. Zhu, J. C. Zhao, Z. F. Zheng, X. P. Gao, *Angew. Chem. Int. Ed.* **2008**, *47*, 5353.

[48] A. S. De Silva Indrasekara, S. J. Norton, N. K. Geitner, B. M. Crawford, M. R. Wiesner, T. Vo-Dinh, *Langmuir* **2018**, *34*, 14617.

[49] C. S. Wagner, S. Shehata, K. Henzler, J. Yuan, A. Wittemann, *J. Colloid Interface Sci.* **2011**, *355*, 115.

[50] R. G. Parkhomenko, A. I. Plekhanov, A. S. Kuchyanov, S. V. Trubin, B. M. Kuchumov, I. K. Igumenov, *Surf. Coatings Technol.* **2013**, *230*, 279.

[51] G. Chu, X. Wang, H. Yin, Y. Shi, H. Jiang, T. Chen, J. Gao, D. Qu, Y. Xu, D. Ding, *ACS Appl. Mater. Interfaces* **2015**, *7*, 21797.

[52] M. N. Hedhili, Z. Zhang, L. Zhang, P. Wang, H. Zhang, *Nano Lett.* **2012**, *13*, 14.

[53] A. B. Tesler, B. M. Maoz, Y. Feldman, A. Vaskevich, I. Rubinstein, *J. Phys. Chem. C* **2013**, *117*, 11337.

[54] A. L. Giermann, C. V. Thompson, *Appl. Phys. Lett.* **2005**, *86*, 1.

[55] J. Wang, M. Jin, Y. Gong, H. Li, S. Wu, Z. Zhang, G. Zhou, L. Shui, J. C. T. Eijkel, A. Van Den Berg, *Lab Chip* **2017**, *17*, 1970.

[56] L. J. De Vreede, A. Van Den Berg, J. C. T. Eijkel, *Nano Lett.* **2015**, *15*, 727.

[57] R. Verdoold, R. Gill, F. Ungureanu, R. Molenaar, R. P. H. Kooyman, *Biosens. Bioelectron.* **2011**, *27*, 77.

[58] E. Saiz, A. P. Tomsia, R. M. Cannon, *Acta Mater.* **1998**, *46*, 2349.

[59] C. M. Müller, F. C. F. Mornaghini, R. Spolenak, *Nanotechnology* **2008**, *19*, 485306.

[60] L. Jiang, W. Wang, H. Fuchs, L. Chi, *Small* **2009**, *5*, 2819.

[61] J. Hou, M. Li, Y. Song, *Angew. Chem. Int. Ed.* **2018**, *57*, 2544.

[62] V. Flauraud, M. Reyes, R. Paniagua-Domínguez, A. I. Kuznetsov, J. Brugger, *ACS Photonics* **2017**, *4*, 1913.

[63] G. Mayonado, S. M. Mian, V. Robbiano, F. Cacialli, *Am. Assoc. Phy.* **2015**, 60.

[64] V. Morandi, F. Marabelli, V. Amendola, M. Meneghetti, D. Comoretto, *Adv. Funct. Mater.* **2007**, *17*, 2779.

[65] R. L. Olmon, B. Slovick, T. W. Johnson, D. Shelton, S. H. Oh, G. D. Boreman, M. B. Raschke, *Phys. Rev. B* **2012**, *86*, 235147.

[66] D. D. E. J. and G. Chumanov, *ChemPhysChem* **2005**, *6*, 1221.

[67] B. J. Messinger, K. U. Von Raben, R. K. Chang, P. W. Barber, *Phys. Rev. B* **1981**, *24*, 649.

[68] C. Burda, X. Chen, R. Narayanan, M. A. El-Sayed, *Chem. Rev.* **2005**, *105*, 1025.

[69] S. Zauscher, D. R. Smith, R. T. Hill, J. J. Mock, A. Chilkoti, A. Degiron, *Nano Lett.* **2008**, *8*, 2245.

[70] A. S. Roberts, A. Pors, O. Albrektsen, S. I. Bozhevolnyi, *Nano Lett.* **2014**, *14*, 783.

[71] A. Li, X. Zhao, S. Anderson, X. Zhang, *Small* **2018**, *14*, 1.

[72] M. Grzelczak, J. Vermant, E. M. Furst, L. M. Liz-marza, *ACS Nano* **2010**, *4*, 3591.

Table of Content

Three-tier spherical photonic crystals with multi-scale tailorable structures are fabricated via droplet confined colloid assembly and metal film dewetting method, showing tunable optical properties of photonic stop band and surface plasmon resonance. Their dual-tunability in optical properties achieved by the 2nd-tier silica nanoparticle patterns and the 3rd-tier plasmonic Au nanocrystal arrays, enables the application for constructing flexible anticounterfeiting films.